12-13-2020

Bone health assessment via digital wrist tomosynthesis in the mammography setting

Yener N. Yeni
Henry Ford Health, YYENI1@hfhs.org

Daniel Oravec
Henry Ford Health, DORAVEC1@hfhs.org

Joshua Drost
Henry Ford Health, jdrost1@hfhs.org

Nicholas Bevins
Henry Ford Health, nickb@rad.hfh.edu

Courtney Morrison
Henry Ford Health, courtneym@rad.hfh.edu

See next page for additional authors

Recommended Citation

Yeni YN, Oravec D, Drost J, Bevins N, Morrison C, and Flynn MJ. Bone health assessment via digital wrist tomosynthesis in the mammography setting. Bone 2020; 144:115804.

Authors
Yener N. Yeni, Daniel Oravec, Joshua Drost, Nicholas Bevins, Courtney Morrison, and Michael J. Flynn

Bone 144 (2021) 115804

Contents lists available at ScienceDirect

Bone

journal homepage: www.elsevier.com/locate/bone

Bone health assessment via digital wrist tomosynthesis in the mammography setting

Yener N. Yeni [a,*], Daniel Oravec [a], Joshua Drost [a], Nicholas Bevins [b], Courtney Morrison [b], Michael J. Flynn [b]

[a] Bone and Joint Center, Henry Ford Health System, Detroit, MI, USA
[b] Department of Radiology, Henry Ford Health System, Detroit, MI, USA

ARTICLE INFO

Keywords:
Osteoporosis diagnosis
Bone quality assessment
Screening prevalence
Digital tomosynthesis imaging
Distal forearm
Breast exam workflow

ABSTRACT

Bone fractures attributable to osteoporosis are a significant problem. Though preventative treatment options are available for individuals who are at risk of a fracture, a substantial number of these individuals are not identified due to lack of adherence to bone screening recommendations. The issue is further complicated as standard diagnosis of osteoporosis is based on bone mineral density (BMD) derived from dual energy x-ray absorptiometry (DXA), which, while helpful in identifying many at risk, is limited in fully predicting risk of fracture. It is reasonable to expect that bone screening would become more prevalent and efficacious if offered in coordination with digital breast tomosynthesis (DBT) exams, provided that osteoporosis can be assessed using a DBT modality. Therefore, the objective of the current study was to explore the feasibility of using digital tomosynthesis imaging in a mammography setting. To this end, we measured density, cortical thickness and microstructural properties of the wrist bone, correlated these to reference measurements from microcomputed tomography and DXA, demonstrated the application in vivo in a small group of participants, and determined the repeatability of the measurements.

We found that measurements from digital wrist tomosynthesis (DWT) imaging with a DBT scanner were highly repeatable ex vivo (error = 0.05%–9.62%) and in vivo (error = 0.06%–10.2%). In ex vivo trials, DWT derived BMDs were strongly correlated with reference measurements (R = 0.841–0.980), as were cortical thickness measured at lateral and medial cortices (R = 0.991 and R = 0.959, respectively) and the majority of microstructural measures (R = 0.736–0.991). The measurements were quick and tolerated by human patients with no discomfort, and appeared to be different between young and old participants in a preliminary comparison.

In conclusion, DWT is feasible in a mammography setting, and informative on bone mass, cortical thickness, and microstructural qualities that are known to deteriorate in osteoporosis. To our knowledge, this study represents the first application of DBT for imaging bone. Future clinical studies are needed to further establish the efficacy for diagnosing osteoporosis and predicting risk of fragility fracture using DWT.

1. Introduction

Osteoporosis (OP) is one of the most common diseases affecting aging individuals, and a primary cause for fragility fractures [1]. Effective treatment options exist for individuals at risk of a fragility fracture once they are identified. However, there are at least two major barriers to the identification of at-risk individuals, and consequently, prevention of fracture: 1) A considerable number of patients who are at risk are not receiving bone tests, even after experiencing a fracture [2–4], and 2) standard bone tests based on bone mineral density (BMD) alone, though helpful in identifying many at risk, do not fully predict bone strength or risk of fracture [5,6].

Despite recommendations from the U. S. Preventive Services Task Force and other major professional and healthcare organizations that women aged >65 years (as young as 50 years if they have a major risk factor) should be screened for osteoporosis [7,8], only 8.7% - 38.2% of patients worldwide undergo bone mineral density testing within 2 years of an initial low energy fracture [2–4]. Indeed, the issue of at-risk patients not receiving bone tests has been highlighted as one of the major gaps in the care of osteoporosis, according to a report by the

* Corresponding author at: Integrative Biosciences Center (iBio), 6135 Woodward Ave, Detroit, MI 48202, USA.
E-mail address: yeni@bjc.hfh.edu (Y.N. Yeni).

https://doi.org/10.1016/j.bone.2020.115804
Received 3 September 2020; Received in revised form 5 December 2020; Accepted 10 December 2020
Available online 13 December 2020

International Osteoporosis Foundation [9]. In contrast, adherence to mammography screening is considerably high (76% - 89.1%) in the same age group [10,11]. It is therefore expected that adherence for women's OP screening would be higher if it could be offered during the time of routine breast screening using the same image modality.

We posit that digital tomosynthesis imaging of the wrist at the time of digital breast tomosynthesis (DBT) is well suited for OP screening in a mammography setting. DBT is widely adopted in routine breast cancer screening [12–14]. In fact, the position of the European Society of Breast Imaging (EUSOBI) is that DBT is set to become "routine mammography" in near future [15]. It is reasonable to expect that with increasing adoption of DBT and continued high adherence to breast screening, bone screening would become more prevalent if offered in coordination with DBT breast exams, provided that osteoporosis can be assessed using a DBT modality.

Due to the configuration of the current DBT systems, the forearm is the most suitable site for bone assessment using a DBT system, as it will simply require positioning of the arm in the scanner while standing at the same height for the breast exam. BMD of the forearm, although shown to be reduced in osteoporosis [16–18], has been considered of limited value in predicting fractures of the hip and spine, monitoring treatment efficacy and decision to treat until recently [19–21]. However, with the addition of microstructural and biomechanical information through high-resolution peripheral imaging technologies, views on the value of imaging this site have changed. There is now accumulated evidence that cortical thickness and trabecular microstructural properties of the distal radius based on high resolution peripheral quantitative computed tomography (HR-pQCT) or micro-MRI are different between postmenopausal women with a major osteoporotic fracture and those without [22–24]. Moreover, microstructure and finite element-estimated failure load of the distal radius based on HR-pQCT imaging have been shown to predict incident major osteoporotic fractures independently from BMD and clinical risk factors in men and postmenopausal women [25,26]. As such, assessment of the wrist using a digital breast tomosynthesis scanner offers great value in the management of osteoporosis and fracture risk.

Previous work demonstrated that digital tomosynthesis (DTS) has sufficient resolution to extract useful textural information from bone images. For example, cancellous bone texture derived from whole body DTS imaging provides variables that can be used to predict vertebral cancellous bone stiffness [27,28] as well as vertebral and hip strength [29,30], and discriminate between individuals with and without a prevalent vertebral fracture [31]. DTS scanners used for breast imaging have even higher resolution than whole body tomosynthesis scanners (100 vs 150–300 μm). As such, we hypothesize that digital wrist tomosynthesis (DWT) is capable of providing detailed information on the quantity, cancellous microstructure, and cortical thickness of distal radial bone. Therefore, the objective of this work was to examine the feasibility of these measurements using ex vivo and in vivo DWT images of human radii. In this work, we document the repeatability of each measurement, determine preliminary correlations between DWT and reference measurements, and observe patient experience to guide future applications.

2. Methods

2.1. Ex vivo studies

Five fresh-frozen right cadaveric forearms (unknown sex and age, deidentified) were acquired from local tissue banks and scanned in a clinical DXA scanner (Hologic Horizon A) using a distal radius protocol to establish a bone density reference. 1/3 distal, mid-distal and ultra-distal radius BMD (DXA-$BMD_{1/3}$, DXA-BMD_{mid} and DXA-BMD_{UD}, respectively) were calculated within the DXA software (APEX v5.6.0.5) using standard regions of interest (ROIs) [32] (Fig. 1). Each forearm was then scanned in a clinical DBT scanner (GE Senographe Essential with Senoclaire) 3 times with repositioning. Nine projection images were acquired over a 25 degree sweep in the medial-lateral direction in a step-and-shoot motion. Acquisitions were performed at 5.2 mAs (35 kV and 51 mA) using a rhodium filter and target. Images were reconstructed at 0.1 × 0.1 mm pixel size in the frontal plane with 1 mm plane thickness.

For calculation of DWT derived BMD analogs, the tomosynthesis image stack was synthesized into a 2D image, similar to DXA (Fig. 1). BMD analogs were calculated by summing intensity values in the 2D image and dividing by the total area for ROIs defined identically to DXA (DWT-$BMD_{1/3}$, DWT-BMD_{mid} and DWT-BMD_{UD}, respectively).

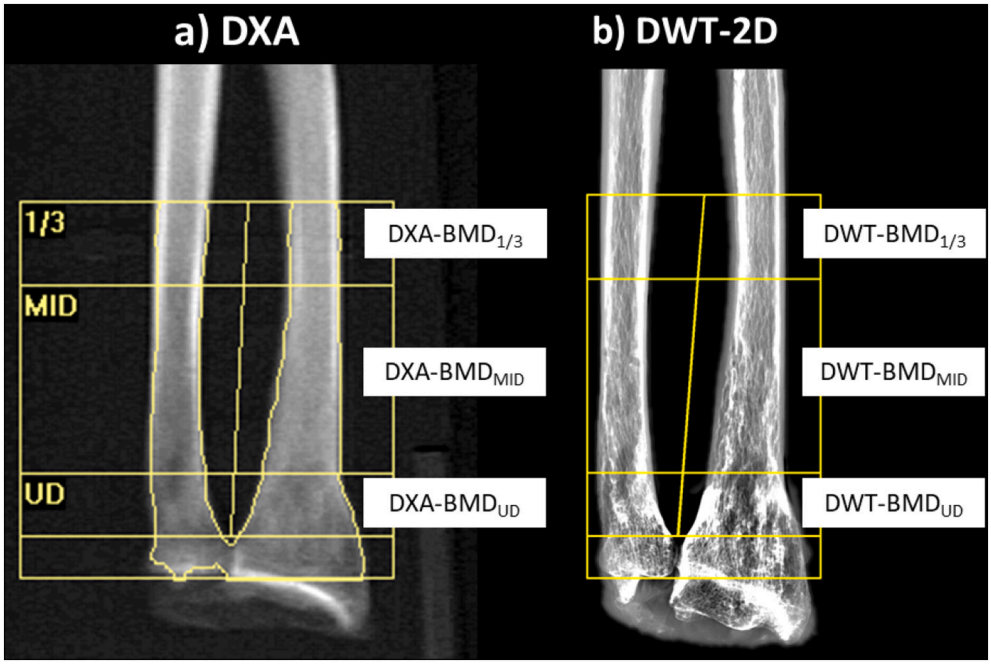

Fig. 1. a) Standard regions of interest in the DXA distal forearm protocol from which DXA-BMDs are measured, and b) the corresponding ROIs in the 2D-synthesized DWT image from which DWT-BMDs were measured.

Alternatively, for the cancellous-rich ultradistal region, we calculated an integral bone volume fraction (iBV/TV) that included both cancellous and cortical bones of the ultradistal region. In calculation of iBV/TV, DWT image volumes were first resampled to isotropic voxel size using bicubic interpolation. Resampled images were then pre-processed using a contrast limited adaptive histogram equalization (CLAHE) algorithm to aid in segmentation (block size = 40, bins = 256, maximum slope = 3) [33]. Briefly, the CLAHE algorithm enhances local contrast by adjusting the gray value at a given voxel using an intensity transformation function based on adjacent voxel values. Total volume (TV) was calculated as the sum of bone voxels after thresholding the 3D image (Otsu method) and closing pores in the structure to delineate the cortical surface [34]. Integral (cancellous and cortical) bone volume (BV) was calculated as the sum of bone voxels after a fixed global threshold was applied. iBV/TV was thus the ratio of BV to TV.

For reference measurements of cortical thickness and microstructure, the radii were scanned using a custom μCT system [35,36] and reconstructed at an isotropic voxel size of 63 μm. Regions for cortical thickness analysis were identified at 50 mm proximal to the distal tip of the radiocarpal joint articular surface (Fig. 2). A 5 mm cross-section was cropped from the axial μCT images centered at the 50 mm plane. The image volume was then binarized to separate bone from background using the Otsu method. Local thickness was calculated within the bone phase of the binarized analysis volume using a sphere fitting algorithm. Cortical thickness (C.Th) was calculated for the lateral and medial cortices contained within a 45 degree wedge volume with its apex at the center of mass of the binarized image in FIJI [37]. For DWT images, the 50 mm analysis regions were identified similarly as described for μCT images. A line profile averaged over 5 mm width drawn perpendicular to the long axis of the radius at the 50 mm location at both medial and lateral cortices was used to calculate cortical bone thickness. Briefly, the periosteal surface was defined as the peak rate of change in gray values along the line profile. The endosteal surface was determined as the last maximum point in the line profile. Cortical thickness was calculated as the difference in mm between the surfaces.

For microstructural analysis of cancellous bone, an analysis volume was selected within the distal radius using the epiphyseal scar, and lateral/medial cortices as corner landmarks (Fig. 2). Analysis volumes were resampled to isotropic voxel size by scaling the depth direction (anterior-posterior direction, 1 mm slices) to match the 100 μm in-plane (lateral-medial) pixel size. Images were then pre-processed to enhance local contrast using CLAHE. Finally, the analysis volumes were binarized either by applying a global threshold value determined by the Otsu method, or alternatively, using the Niblack local thresholding method [38] in FIJI (radius = 15, $k = 0.2$, $C = 0$). Briefly, the Niblack method compares the value at a given voxel to its vicinity. If the voxel in question has a value greater than the mean plus a constant k times the standard deviation of adjacent voxels, that voxel is considered within the bone phase. The two thresholding methods were chosen to extract different aspects of the microstructure. Namely, global thresholding emphasized large features (akin to a low-pass filter), and local thresholding preserved fine detail in trabecular structure (akin to a high-pass filter) (Fig. 3). Trabecular volume fraction (BV/TV), thickness (Tb.Th), number (Tb.N), separation (Tb.Sp), connectivity (Conn.Dn)), anisotropy (DA) and fractal dimension (3D FD) were calculated in CTan (Bruker, Belgium) [39] for the 3D binarized volumes from DWT and μCT.

In addition to standard stereological parameters, average fractal (2D FD, λ and S_λ) parameters (Table 1) for cancellous bone were calculated for the DWT volume using the FracLac plug-in of ImageJ (NIH, MD) [37,40]. Orientation as measured by line fraction deviation (LFD) was calculated as described previously for vertebral images from whole body tomosynthesis [27,29]. Fractal dimension (FD) and lacunarity (λ) are common measures of complexity where simple morphometric measures are not feasible or adequate for describing microstructure. Fractal dimension defines roughness of texture and is strongly associated with BV/TV in cancellous bone [41,42]. Lacunarity measures pore size distributions and thus λ and scale-dependent lacunarity (S_λ) measure tissue heterogeneity [43].

Precision error was characterized using the root mean square coefficient of variation (%CV_{rms}) of repeated measurements [44]. The DWT-BMDs and iBV/TV from DWT were correlated to DXA measurements on a regional basis. Cortical thickness and microstructural variables were correlated to μCT measurements from the corresponding ROIs.

2.2. *In vivo studies*

In order to demonstrate the feasibility of assessing bone health using a breast tomosynthesis scanner in live humans, 5 female patients (ages 19–76) were enrolled under institutional approval and informed consent. Patients were instructed to align their nondominant hand (all right-handed) on a generic hand template taped to the imaging platform, with the elbow flexed and hand in the dorso-palmar view (Fig. 4). Tomosynthesis images were acquired three times with repositioning (radiographic technique and analysis methods same as ex vivo studies).

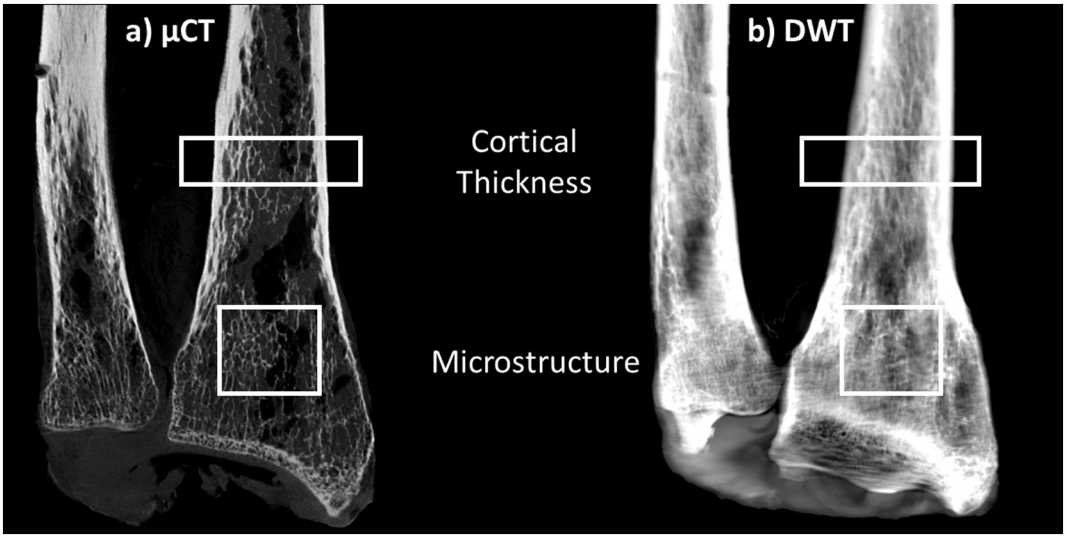

Fig. 2. a) μCT image of the distal forearm bones with the regions of interests for cortical thickness and microstructure measurements and b) the corresponding ROIs in the DWT image.

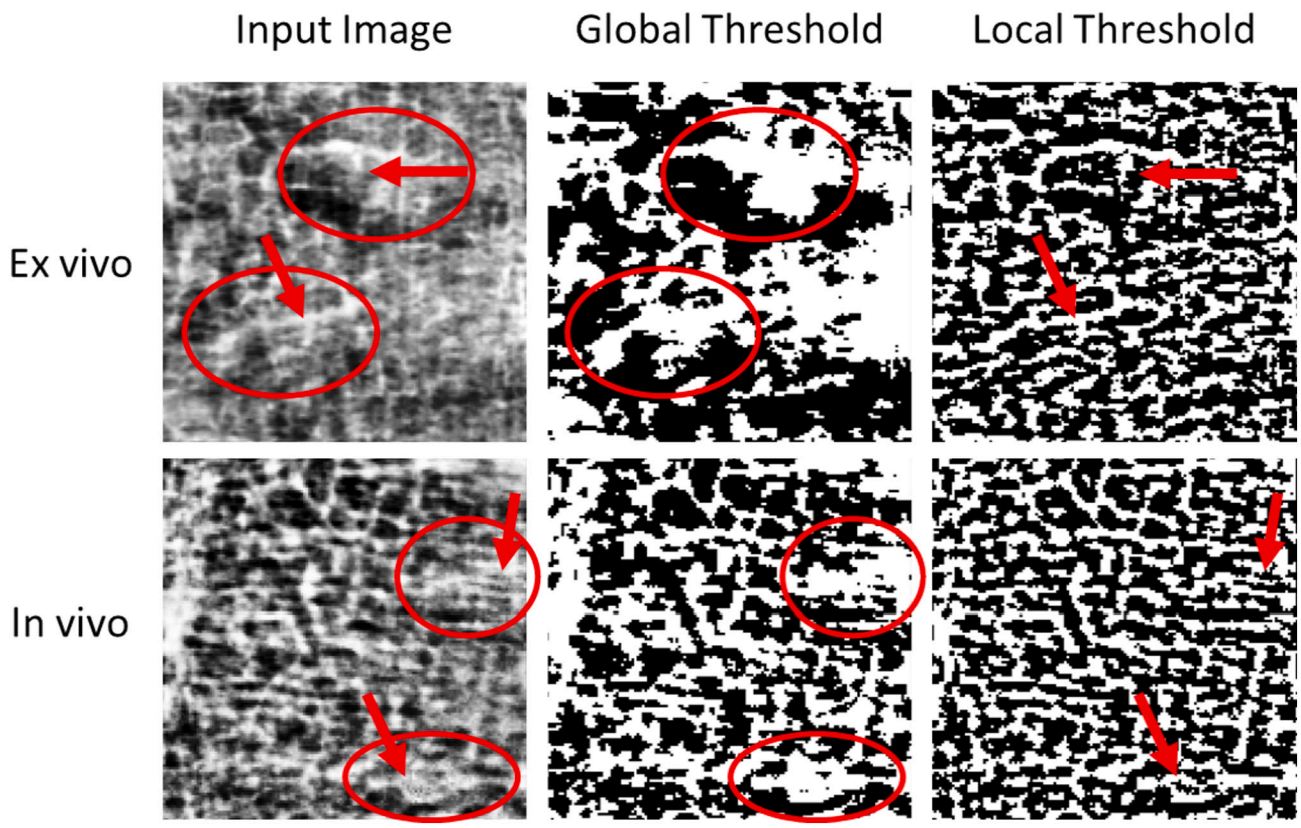

Fig. 3. DWT analysis regions (left column) from ex vivo (cadaveric wrist, top row) and in vivo (study participant, bottom row) images were pre-processed using CLAHE and binarized using two thresholding methods: Otsu global thresholding (center column) and Niblack local thresholding method (right column). The global thresholding method emphasized large microstructural features (examples encircled) while the local method extracted fine features (examples indicated with arrows).

DWT-BMDs, iBV/TV, cortical thickness, microstructural variables, and associated precision errors were characterized as described for the ex vivo studies. Although not the primary interest with this small sample, differences between young and old participants (Young:19, 34, 34 yrs.; Old:59, 76 yrs) were examined using *t*-tests to gain a preliminary insight into which variables are potentially sensitive to age-related differences as captured on DWT. The first set of measurements (one data point per patient) were used for this purpose.

Dosimetry measurements were performed in preparation of the in vivo studies by measuring the entrance skin exposure (ESE) using a solid state dosimeter (Accu-Gold+, Radcal) positioned approximately at the position of the entrance surface of a wrist (4.5 cm from the imaging platform). The dosimeter reading was converted to effective dose using conversion factor of 0.46 μSv/mGy [45].

3. Results

3.1. Ex vivo

The precision error was 0.05% to 9.62% for DWT measurements (Table 1). DWT derived BMDs and iBV/TV were strongly correlated to BMDs from DXA (Table 1, Fig. 5), and DWT derived C.Th was strongly correlated to that from μCT (Table 1, Fig. 6). A majority of microstructural measures were strongly and positively correlated ($R > 0.7$) to the μCT references, except for connectivity density which had a negative correlation with μCT (Table 1, Fig. 7). For microstructural variables, images processed using local thresholding demonstrated slightly stronger correlations with μCT (R values up to 0.98, Table 1) than those processed using global thresholding (R values up to 0.90).

3.2. In vivo

The resultant effective dose for each tomosynthesis acquisition was 8.9 μSv. Patients or technical staff had no difficulty with the imaging protocol. The entire session was approximately 4 min from entering to exiting the room, with image acquisition constituting approximately 9 s for each of 3 trials. The precision error ($\%CV_{RMS}$) from three trials with repositioning was 0.06% to 10.2% for DWT derived measurements (Table 2). We observed that iBV/TV and several microstructural variables might be associated with patient age (Young:19, 34, 34 yrs.; Old:59, 76 yrs) based on *t*-tests (Table 2). For microstructural variables, images processed using global thresholding demonstrated potentially stronger associations with patient age ($p = 0.017$–0.484, Table 2) than those processed using local thresholding ($p = 0.034$–0.593).

4. Discussion

This study examined the feasibility of conducting bone health screening in the clinical breast tomosynthesis setting. To that end, we determined the ex vivo and in vivo repeatability of commonly recognized metrics of bone quantity, cortical thickness and microstructure. In addition, we determined preliminary correlations between tomosynthesis derived metrics and reference measurements. The findings are supportive of further development of this approach. To our knowledge, this study represents the first use of a breast tomosynthesis scanner in assessment of bone qualities.

The procedure was tolerated without discomfort for in vivo trials. Effective radiation dose estimated from dosimetry measurements (8.9 μSv) was a fraction of the radiation exposure of a CT exam [46–48] with exposure comparable to a standard radiographic examination [49–51].

Table 1
Ex vivo repeatability (%CV_{RMS}) of DWT derived BMD, cortical thickness and cancellous bone microstructural metrics, and their correlation (R) with the corresponding reference measurements. DWT data are reported from images processed using the local thresholding method.

Var. type	DWT variable	Variable name/interpretation	%CV_{RMS}	R
BMD	DWT-$BMD_{1/3}$	1/3 radius BMD	0.85	0.841
	DWT-BMD_{mid}	Mid radius BMD	0.78	0.970
	DWT-BMD_{UD}	Ultradistal radius BMD	0.50	0.980
	iBV/TV	Ultradistal integral bone volume fraction	1.39	0.982[a]
Cancellous μStructure	BV/TV	Bone volume fraction	0.66	0.959
	Tb.Th	Trabecular thickness	0.53	0.394[b]
	Tb.N	Trabecular number	0.43	0.915
	Tb.Sp	Trabecular separation	0.91	0.983
	Conn.Dn	Connectivity density	4.50	−0.493
	DA	3D Degree of anisotropy	1.80	0.915
	LFD	Line fraction deviation (Tr. Orientation)	3.53	*N/A*
	3D FD	Fractal dimension (Complexity) – 3D Binary	0.06	0.736
	2D FD	Fractal dimension (Complexity) – 2D Gray Level	0.05	*N/A*
	λ	Lacunarity (Heterogeneity)	0.90	*N/A*
	$S_λ$	Lacunarity/Sizescale (Heterogeneity)	1.36	*N/A*
Cortical thickness	C.Th.L	Lateral cortical thickness	4.66	0.991
	C.Th.M	Medial cortical thickness	9.62	0.959

[a] Correlation to DXA-BMD_{UD}. [b] Correlation is 0.775 using the global (coarser) threshold technique. N/A: Not available for μCT; Note $p < 0.05$ for $R > 0.878$; $p < 0.10$ for $R > 0.805$.

Acquisition time (approximately 9 s) was short compared to peripheral CT imaging, which can take several minutes [52,53]. Thus, DWT does not increase concern with radiation exposure or image acquisition time associated with bone screening.

Precision of bone mass measures derived from DWT ex vivo (0.50–1.39%) and in vivo (0.29–3.14%) is comparable to the in vivo values previously reported for distal and ultradistal BMD measures using single- (0.7–1.6%) and dual-energy absorptiometry (DXA) (1.1–2.9%) [54]. Precision of cortical thickness and microstructural parameters derived from DWT ex vivo and in vivo is also well within the range of that derived from HR-pQCT of the wrist ex vivo [55] and in vivo [22,52,56], respectively. As such, DWT offers sufficient repeatability for measuring bone properties.

DWT derived bone mass, cortical thickness, and microstructural measures were strongly correlated to those measured from DXA and μCT. The correlations of DWT-BMD_{mid} DWT-BMD_{UD}, iBV/TV and C.Th with the corresponding reference measurements were high enough to reach a level of $p < 0.05$ with the small sample. A majority of microstructural measures were strongly and positively correlated ($R > 0.7$) to the μCT references, with BV/TV, Tb.N, Tb.Sp and DA reaching a statistically demonstrable level. Failure to find the expected correlation with reference measurements for connectivity might be attributable to the strong 3D nature of this property and poor resolution of DWT in one direction (dorso-palmar in the current protocol). However, anisotropic resolution is typical of many clinical systems and is not a limitation specific to DWT. Nevertheless, among the geometric and cancellous microstructural variables measurable from the wrist, C.Th, BV/TV, Tb.Th, Tb.N, Tb.Sp and fractal dimension have been shown to be associated with major osteoporotic fractures [22,23,57]. Consistent with these reports, iBV/TV, Tb.Th, Tb.N, Tb.Sp and fractal dimension present as different between young and old women in our preliminary demonstration; an observation suggesting potential utility for these DWT variables.

Segmentation of cancellous and binarization of the segmented image is necessary for analysis of bone microstructure. In this work, we evaluated two common approaches for image binarization. It was noted that global thresholding generally represented a qualitatively conservative binarization approach and captured larger features of cancellous microstructure (Fig. 3). Local thresholding facilitated a more aggressive binarization, and extracted fine detail within regions of similar intensity value. Not surprisingly, correlations between DWT and μCT were stronger when binarized using local thresholding methods (Table 1,

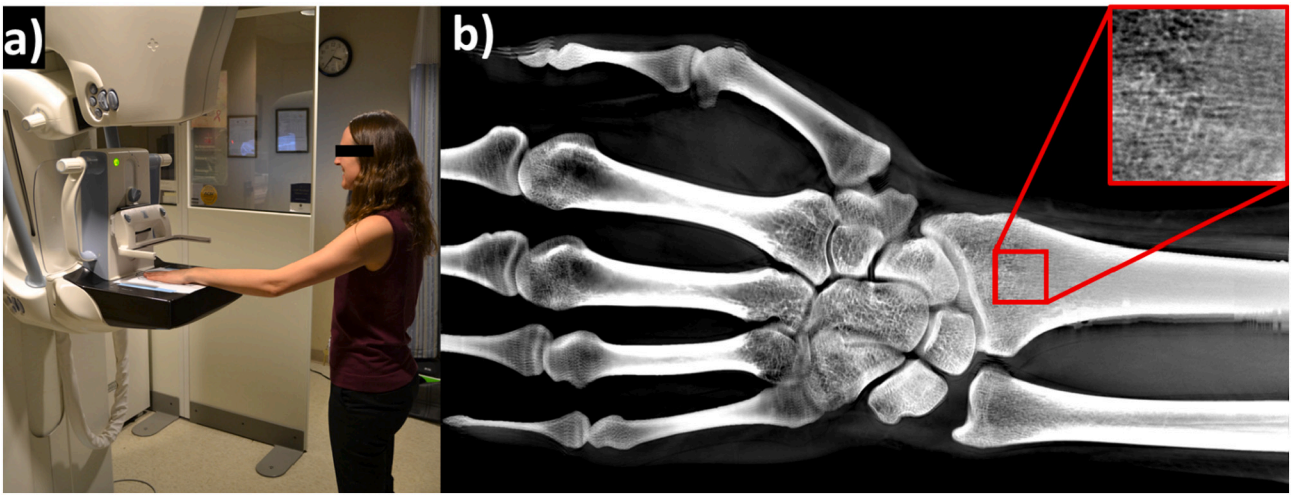

Fig. 4. a) DWT imaging using a digital breast tomosynthesis scanner, and b) DWT image of the wrist from a 19 year old woman. Minute details of the cortical and cancellous structure are clearly visible.

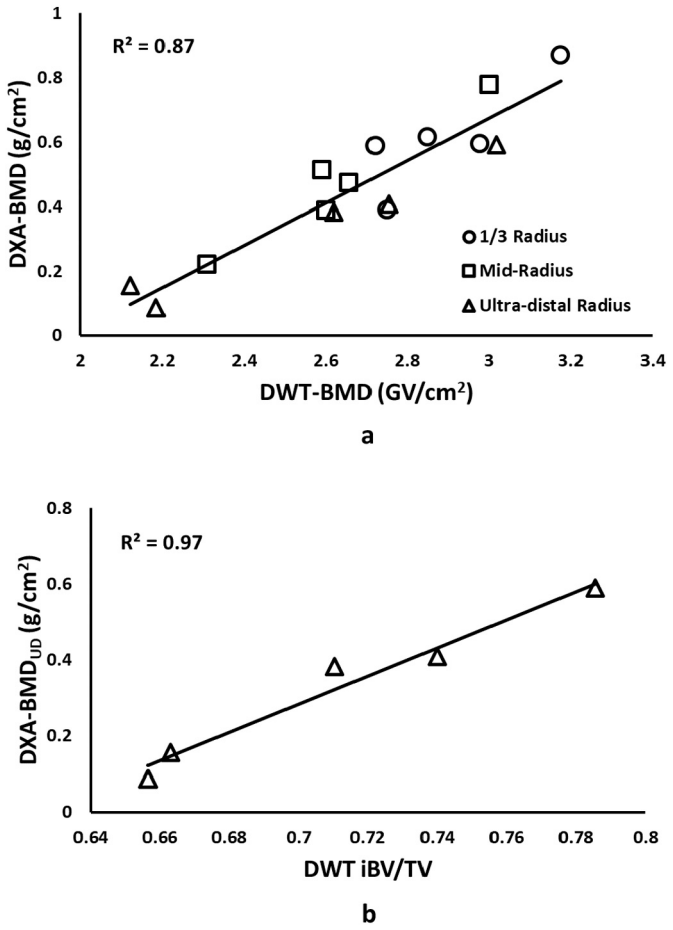

Fig. 5. a) 1/3-, mid- and ultradistal BMD measured from DXA (units: grams per square centimeter, g/cm^2) are strongly correlated with the respective measurements from DWT (Table 1, units: gray value per square centimeter, GV/cm^2), giving an R^2 of 0.87 for pooled regions. b) The integral BV/TV of the ultradistal radius measured from DWT was also strongly correlated to ultradistal BMD from DXA.

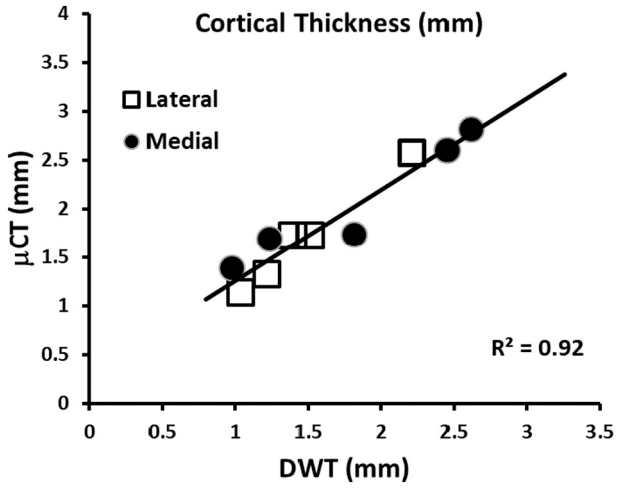

Fig. 6. Cortical thicknesses measured from lateral and medial cortices are strongly correlated between µCT and DWT ($R^2 = 0.98$ and $R^2 = 0.92$, respectively), giving an R^2 of 0.92 for pooled cortices.

Fig. 7) which, like µCT, retain fine detail. However, we observed that microstructural variables might be more distinctly separated by age in vivo when derived from globally thresholded images (Table 2). It is possible that age-related changes in trabecular architecture may be more accurately identified in gross features, however, this remains to be a speculation until confirmed in a larger patient sample. Although this work is a preliminary demonstration of an envisioned image processing workflow, the current results emphasize the importance of careful consideration of segmentation methods for successful assessment of cancellous bone microstructure.

Central DXA is the most commonly used screening test, and BMD from central DXA (i.e., that of hip and spine) is most commonly used in treatment guidelines, although BMD of distal forearm is recognized to have similar accuracy to that of central DXA [8]. As such, a testing modality aiming to increase screening prevalence should ideally provide BMD or a bone metric that is analogous to BMD, for easier interpretation and translation of this modality. Therefore, in moving forward, calibrating the DWT-BMDs to DXA derived BMDs would be important. The calculation of iBV/TV is different from that of DWT-BMDs in terms of image reconstruction (3D vs 2D synthesis) and processing (binary vs gray level). iBV/TV therefore offers an alternative calculation of bone mass, should gray level calculations from 2D synthesized images prove problematic in future. Correlations of HR-pQCT derived radial volumetric BMD and BV/TV with spine and hip BMDs [22] are similar to that of DWT derived iBV/TV with DXA derived ultradistal BMD in the current study. This suggests iBV/TV as a potentially useful BMD analog. It was also more sensitive than DWT-BMDs to age difference in our small cohort. Therefore, we consider iBV/TV in the category of BMD or generally bone quantity variables to be explored further in relationship with hip and spine DXA measurements. If the information obtained via DWT is limited to the wrist, this may still be useful in assessing the risk of wrist fracture [58]. A prior wrist fracture significantly increases the risk of any subsequent fragility fracture independently from baseline BMD and common osteoporotic risk factors [59–61]. Therefore, identification of individuals at risk of a forearm fragility fracture based on DWT would allow for a timely decision for intervention to prevent fragility fractures at other sites.

Owing to the current role of DBT in breast screening, the DWT modality is expected to be widely available, accessible and visible. Therefore, if the DWT derived BMD analogs presented here are equally effective as DXA derived BMD based screening, as the results suggest, the presented DWT approach is expected to be highly translational and scalable. This is a significant advantage over screening efforts aiming to use standalone imaging modalities, including the relatively less common whole body DTS scanners for bone health assessment [30,31]. DWT based bone assessment is also expected to benefit patients other than those routinely screened for postmenopausal osteoporosis. For example, treatment-related bone loss and bone maintenance in breast cancer survivors are well-known issues in breast cancer [62,63]. Periodic post-treatment surveillance via mammography is highly recommended by major institutions including American Society of Clinical Oncology, European Society of Medical Oncology and National Comprehensive Cancer Network [64–66]. As such, DWT imaging that is readily available at the time of surveillance may be efficient for monitoring changes in bone health associated with cancer and bone therapy.

There are also challenges associated with imaging of hip or spine, or using other modalities for obese patients due to physical constraints of the imaging system and also due to inaccurate readings resulting from excessive soft tissue [67–69]. The DWT approach would utilize a system that images the wrist while the patient is standing outside of the imaging modality. In turn, concerns about excessive soft tissue would be reduced, potentially allowing for a screening process that can be standardized to include obese patients.

The DWT based approach for bone screening in the mammography setting is ideally suited for women. The technique may be less beneficial for men in terms of screening prevalence, if DWT is only as effective as

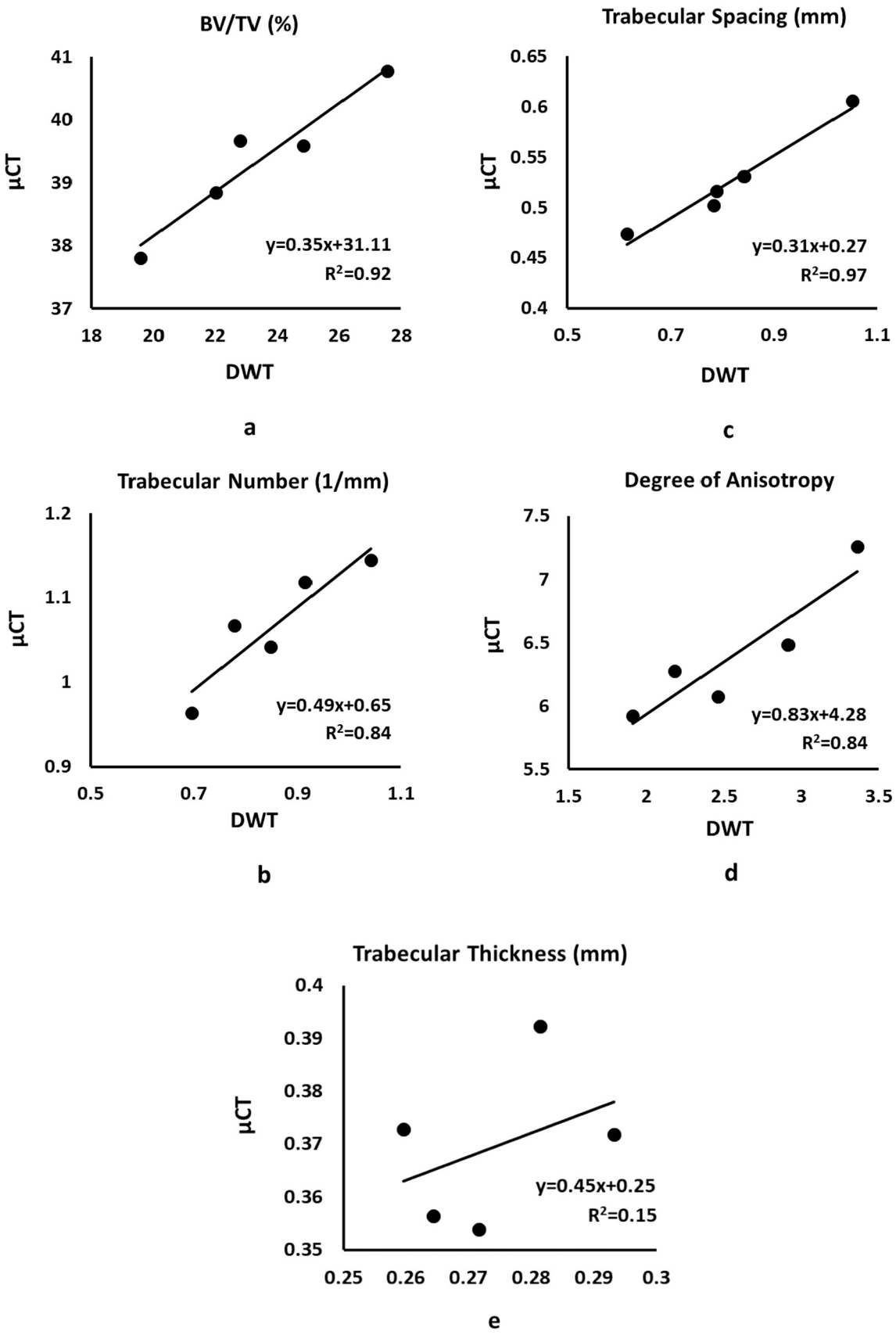

Fig. 7. The relationship between μCT and DWT for a) Trabecular bone volume fraction, b) trabecular number, c) trabecular separation, d) degree of anisotropy, and e) trabecular thickness, as determined from images binarized using local thresholding.

Table 2
In vivo repeatability (%CV_{RMS}) of DWT derived BMD, cortical thickness and cancellous bone microstructural metrics. DWT data are reported from images processed using the global thresholding method.

Variable	%CV_{RMS}	Descriptive Old; Young (av ± sd)	p-value
DWT-$BMD_{1/3}$	N/A	N/A	N/A
DWT-BMD_{mid}	0.29	3907.3 ± 49.8, 3897.1 ± 16.5	0.822
DWT-BMD_{UD}	0.91	3583.2 ± 285.9, 3553.4 ± 86.7	0.908
iBV/TV	**3.14**	**0.451 ± 0.014, 0.545 ± 0.033**	**0.025**
BV/TV	1.32	50.2 ± 2.0, 51.9 ± 3.0	0.484
Tb.Th	**2.52**	**0.781 ± 0.032, 0.609 ± 0.041**	**0.017**
Tb.N	**2.35**	**0.642 ± 0.001, 0.855 ± 0.054**	**0.021**
Tb.Sp	**1.76**	**0.740 ± 0.010, 0.555 ± 0.071**	**0.043**
Conn.Dn	6.02	0.344 ± 0.061, 0.622 ± 0.133	0.054
DA	1.57	5.93 ± 0.16, 7.06 ± 0.58	0.066
LFD	**3.34**	**1.18 ± 0.08, 0.66 ± 0.08**	**0.012**
3D FD	**0.36**	**2.672 ± 0.007, 2.733 ± 0.010**	**0.005**
2D FD	0.06	2.770 ± 0.044, 2.787 ± 0.011	0.691
λ	3.36	0.072 ± 0.003, 0.077 ± 0.019	0.717
$S_λ$	**2.12**	**0.067 ± 0.001, 0.072 ± 0.001**	**0.008**
C.Th.L	8.8	2.79 ± 0.44, 3.29 ± 0.23	0.328
C.Th.M	10.2	4.16 ± 0.42, 3.17 ± 0.57	0.118

N/A: Not available.

DXA-BMD. However, there is technically no difficulty in scanning men using the DWT modality, and it can be offered as an alternative to men. If the additional cortical thickness and microstructural metrics increase the accuracy of fracture risk assessment over BMD alone, DWT could be of direct benefit to men as well. For this reason, future studies should consider inclusion of men.

Although the quantitative diagnostic standard has been based on BMD, DXA images can be used to derive a textural measure called trabecular bone score (TBS). TBS is a gray-level measure of microstructural heterogeneity in tissue organization and considered to enhance prediction of fracture risk [70–72]. The ISCD's official position is that TBS can be used to adjust fracture probability in risk assessment tools [20]. As such, in identifying microstructural variables that can enhance fracture risk prediction over BMD alone, examining the extent to which they fill the same niche as TBS should be considered in future studies.

Recent peripheral scanning approaches focus on distal tibia in addition to the forearm [22,23]. It is possible to scan distal tibia in a DWT modality, however, this would require less comfortable positioning for the patient, and potential addition of a scan bed into the exam environment which would affect logistics. If the superiority of distal tibia over forearm for osteoporosis and fracture risk assessment becomes well-established, this mode of imaging through a breast scanner, or a modification to scanner geometry could be explored.

In addition to the limitations discussed above, a major limitation of this study is the small sample. While the sample is considered adequate for repeatability calculations [44] and demonstration of in vivo applicability, the correlations between DWT and reference modalities, though promising, must be considered as preliminary. Likewise, separation of DWT variables by age must be considered a preliminary screening of data for consistency with the literature. The *p*-values for age comparisons are provided as a guideline in identifying variables of potential utility. Nonetheless, the data are considered useful for descriptive purposes, future designs and also for highlighting the potential importance of image processing approaches in the DWT outcomes. In addition, patient age cannot be equated to osteoporosis status. As such, the next steps of this research would involve designing an adequately powered case-control study to establish the ability of DWT to discriminate osteoporotic patients from normal controls using DXA T-scores as the reference.

In summary, this study presents methods for analysis of distal radius bone using a breast tomosynthesis imaging system to derive parameters that are interpretable in terms of established metrics for bone density, cortical thickness, and cancellous bone microstructure. These methods are repeatable and applicable to live humans without difficulty. Although preliminary in nature due to small sample, the DWT derived parameters had large correlations with those from reference modalities. Collectively, these results demonstrate the feasibility of bone health assessment using a breast tomosynthesis scanner, and support further development of DWT based criteria that can be used in osteoporosis screening and fracture risk assessment.

Funding

This research did not receive any specific grant from funding agencies in the public, commercial, or not-for-profit sectors.

CRediT authorship contribution statement

Yener N. Yeni: Conceptualization, Methodology, Validation, Formal analysis, Writing – original draft, Writing – review & editing, Visualization, Supervision, Project administration. **Daniel Oravec:** Methodology, Validation, Investigation, Formal analysis, Data curation, Writing – review & editing, Visualization. **Joshua Drost:** Methodology, Investigation, Data curation, Writing – review & editing. **Nicholas Bevins:** Methodology, Writing – review & editing, Supervision. **Courtney Morrison:** Methodology, Investigation, Writing – review & editing. **Michael J. Flynn:** Conceptualization, Methodology, Writing – review & editing, Supervision.

Declaration of competing interest

None.

References

[1] A. Singer, A. Exuzides, L. Spangler, C. O'Malley, C. Colby, K. Johnston, I. Agodoa, J. Baker, R. Kagan, Burden of illness for osteoporotic fractures compared with other serious diseases among postmenopausal women in the United States, Mayo Clin. Proc. 90 (1) (2015) 53–62.
[2] A. Vanasse, P. Dagenais, T. Niyonsenga, J.P. Gregoire, J. Courteau, A. Hemiari, Bone mineral density measurement and osteoporosis treatment after a fragility fracture in older adults: regional variation and determinants of use in Quebec, BMC Musculoskelet. Disord. 6 (2005) 33.
[3] C. Angthong, S. Rodjanawijitkul, S. Samart, W. Angthong, Prevalence of bone mineral density testing and osteoporosis management following low- and high-energy fractures, Acta Orthop. Traumatol. Turc. 47 (5) (2013) 318–322.
[4] T. Baba, H. Hagino, H. Nonomiya, T. Ikuta, E. Shoda, A. Mogami, T. Sawaguchi, K. Kaneko, Inadequate management for secondary fracture prevention in patients with distal radius fracture by trauma surgeons, Osteoporos. Int. 26 (7) (2015) 1959–1963.
[5] J.A. Kanis, O. Johnell, A. Oden, A. Dawson, C. De Laet, B. Jonsson, Ten year probabilities of osteoporotic fractures according to BMD and diagnostic thresholds, Osteoporos. Int. 12 (12) (2001) 989–995.
[6] A. Cranney, S.A. Jamal, J.F. Tsang, R.G. Josse, W.D. Leslie, Low bone mineral density and fracture burden in postmenopausal women, CMAJ 177 (6) (2007) 575–580.
[7] L.S. Lim, L.J. Hoeksema, K. Sherin, A.P.P. Committee, Screening for osteoporosis in the adult U.S. population: ACPM position statement on preventive practice, Am J Prev Med 36 (4) (2009) 366–375.
[8] S.J. Curry, A.H. Krist, D.K. Owens, M.J. Barry, A.B. Caughey, K.W. Davidson, C. A. Doubeni, J.W. Epling Jr., A.R. Kemper, M. Kubik, C.S. Landefeld, C. M. Mangione, M.G. Phipps, M. Pignone, M. Silverstein, M.A. Simon, C.W. Tseng, J. B. Wong, Screening for osteoporosis to prevent fractures: US preventive services task force recommendation statement, JAMA 319 (24) (2018) 2521–2531.
[9] N. Harvey, E.V. McCloskey, Gaps and Solutions in Bone Health - A Global Framework for Improvement, International Osteoporosis Foundation, 2016.
[10] R.A. Hubbard, E.S. O'Meara, L.M. Henderson, D. Hill, D. Braithwaite, J.S. Haas, C. I. Lee, B.L. Sprague, J. Alford-Teaster, A.N.A. Tosteson, K.J. Wernli, T. Onega, Multilevel factors associated with long-term adherence to screening mammography in older women in the U.S, Prev. Med. 89 (2016) 169–177.
[11] A. Narayan, A. Fischer, Z. Zhang, R. Woods, E. Morris, S. Harvey, Nationwide cross-sectional adherence to mammography screening guidelines: national behavioral risk factor surveillance system survey results, Breast Cancer Res. Treat. 164 (3) (2017) 719–725.
[12] Y. Gao, J.S. Babb, H.K. Toth, L. Moy, S.L. Heller, Digital breast tomosynthesis practice patterns following 2011 FDA approval: a survey of breast imaging radiologists, Acad. Radiol. 24 (8) (2017) 947–953.

[13] L.A. Hardesty, S.M. Kreidler, D.H. Glueck, Digital breast Tomosynthesis utilization in the United States: a survey of physician members of the society of breast imaging, J. Am. Coll. Radiol. 13 (11S) (2016) R67–R73.
[14] R.C. Miles, T. Onega, C.I. Lee, Addressing potential health disparities in the adoption of advanced breast imaging technologies, Acad. Radiol. 25 (5) (2018) 547–551.
[15] F. Sardanelli, H.S. Aase, M. Alvarez, E. Azavedo, H.J. Baarslag, C. Balleyguier, P. A. Baltzer, V. Beslagic, U. Bick, D. Bogdanovic-Stojanovic, R. Briediene, B. Brkljacic, J. Camps Herrero, C. Colin, E. Cornford, J. Danes, G. de Geer, G. Esen, A. Evans, M.H. Fuchsjaeger, F.J. Gilbert, O. Graf, G. Hargaden, T.H. Helbich, S. H. Heywang-Kobrunner, V. Ivanov, A. Jonsson, C.K. Kuhl, E.C. Lisencu, E. Luczynska, R.M. Mann, J.C. Marques, L. Martincich, M. Mortier, M. Muller-Schimpfle, K. Ormandi, P. Panizza, F. Pediconi, R.M. Pijnappel, K. Pinker, T. Rissanen, N. Rotaru, G. Saguatti, T. Sella, J. Slobodnikova, M. Talk, P. Taourel, R.M. Trimboli, I. Vejborg, A. Vourtsis, G. Forrai, Position paper on screening for breast cancer by the European Society of Breast Imaging (EUSOBI) and 30 national breast radiology bodies from Austria, Belgium, Bosnia and Herzegovina, Bulgaria, Croatia, Czech Republic, Denmark, Estonia, Finland, France, Germany, Greece, Hungary, Iceland, Ireland, Italy, Israel, Lithuania, Moldova, The Netherlands, Norway, Poland, Portugal, Romania, Serbia, Slovakia, Spain, Sweden, Switzerland and Turkey, Eur Radiol 27 (7) (2017) 2737–2743.
[16] R. Eastell, B.L. Riggs, H.W. Wahner, W.M. O'Fallon, P.C. Amadio, L.J. Melton 3rd, Colles' fracture and bone density of the ultradistal radius, J. Bone Miner. Res. 4 (4) (1989) 607–613.
[17] H. Mallmin, S. Ljunghall, Distal radius fracture is an early sign of general osteoporosis: bone mass measurements in a population-based study, Osteoporos. Int. 4 (6) (1994) 357–361.
[18] H. Mallmin, S. Ljunghall, T. Naessen, Colles' fracture associated with reduced bone mineral content. Photon densitometry in 74 patients with matched controls, Acta Orthop Scand 63 (5) (1992) 552–554.
[19] S. Grampp, M. Jergas, P. Lang, E. Steiner, T. Fuerst, C.C. Gluer, A. Mathur, H. K. Genant, Quantitative CT assessment of the lumbar spine and radius in patients with osteoporosis, AJR Am. J. Roentgenol. 167 (1) (1996) 133–140.
[20] J.A. Shepherd, J.T. Schousboe, S.B. Broy, K. Engelke, W.D. Leslie, Executive summary of the 2015 ISCD position development conference on advanced measures from DXA and QCT: fracture prediction beyond BMD, J. Clin. Densitom. 18 (3) (2015) 274–286.
[21] M.L. Bouxsein, R.A. Parker, S.L. Greenspan, Forearm bone mineral densitometry cannot be used to monitor response to alendronate therapy in postmenopausal women, Osteoporos. Int. 10 (6) (1999) 505–509.
[22] L. Vico, M. Zouch, A. Amirouche, D. Frere, N. Laroche, B. Koller, A. Laib, T. Thomas, C. Alexandre, High-resolution pQCT analysis at the distal radius and tibia discriminates patients with recent wrist and femoral neck fractures, J. Bone Miner. Res. 23 (11) (2008) 1741–1750.
[23] S. Boutroy, S. Khosla, E. Sornay-Rendu, M.B. Zanchetta, D.J. McMahon, C. A. Zhang, R.D. Chapurlat, J. Zanchetta, E.M. Stein, C. Bogado, S. Majumdar, A. J. Burghardt, E. Shane, Microarchitecture and peripheral BMD are impaired in postmenopausal white women with fracture independently of Total hip T-score: an international multicenter study, J. Bone Miner. Res. 31 (6) (2016) 1158–1166.
[24] R. Kijowski, M. Tuite, D. Kruger, A. Munoz Del Rio, M. Kleerekoper, N. Binkley, Evaluation of trabecular microarchitecture in nonosteoporotic postmenopausal women with and without fracture, J. Bone Miner. Res. 27 (7) (2012) 1494–1500.
[25] L. Langsetmo, K.W. Peters, A.J. Burghardt, K.E. Ensrud, H.A. Fink, P.M. Cawthon, J.A. Cauley, J.T. Schousboe, E. Barrett-Connor, E.S. Orwoll, G. Osteoporotic fractures in men study research, volumetric bone mineral density and failure load of distal limbs predict incident clinical fracture independent HR-pQCT BMD and failure load predicts incident clinical fracture of FRAX and clinical risk factors among older men, J Bone Miner Res 33(7) (2018) 1302–1311.
[26] E. Sornay-Rendu, S. Boutroy, F. Duboeuf, R.D. Chapurlat, Bone microarchitecture assessed by HR-pQCT as predictor of fracture risk in postmenopausal women: the OFELY study, J. Bone Miner. Res. 32 (6) (2017) 1243–1251.
[27] W. Kim, D. Oravec, G.W. Divine, M.J. Flynn, Y.N. Yeni, Effect of view, scan orientation and analysis volume on digital tomosynthesis (DTS) based textural analysis of bone, Ann. Biomed. Eng. 45 (5) (2017) 1236–1246.
[28] W. Kim, D. Oravec, S. Nekkanty, J. Yerramshetty, E.A. Sander, G.W. Divine, M. J. Flynn, Y.N. Yeni, Digital tomosynthesis (DTS) for quantitative assessment of trabecular microstructure in human vertebral bone, Med. Eng. Phys. 37 (1) (2015) 109–120.
[29] Y.N. Yeni, W. Kim, D. Oravec, M. Nixon, G.W. Divine, M.J. Flynn, Assessment of vertebral wedge strength using cancellous textural properties derived from digital tomosynthesis and density properties from dual energy X-ray absorptiometry and high resolution computed tomography, J. Biomech. 79 (2018) 191–197.
[30] M. Fujii, T. Aoki, Y. Okada, H. Mori, S. Kinoshita, Y. Hayashida, M. Hajime, K. Tanaka, Y. Tanaka, Y. Korogi, Prediction of Femoral Neck Strength in Patients with Diabetes Mellitus with Trabecular Bone Analysis and Tomosynthesis Images, Radiology (2016) 151657.
[31] D. Oravec, O. Yaldo, C. Bolton, M.J. Flynn, M. van Holsbeeck, Y.N. Yeni, Digital tomosynthesis and fractal analysis predict prevalent vertebral fractures in patients with multiple myeloma: a preliminary in vivo study, AJR Am. J. Roentgenol. (2019) W1–W7.
[32] J.A. Shepherd, X.G. Cheng, Y. Lu, C. Njeh, J. Toschke, K. Engelke, M. Grigorian, H. K. Genant, Universal standardization of forearm bone densitometry, J. Bone Miner. Res. 17 (4) (2002) 734–745.
[33] K. Zuiderveld, Contrast limited adaptive histogram equalization, in: P.S. Heckbert (Ed.), Graphics Gems IV, Academic Press Professional, Inc, San Diego, CA, 1994, pp. 474–485.
[34] J. Ollion, J. Cochennec, F. Loll, C. Escude, T. Boudier, TANGO: a generic tool for high-throughput 3D image analysis for studying nuclear organization, Bioinformatics 29 (14) (2013) 1840–1841.
[35] D. Oravec, A. Quazi, A. Xiao, E. Yang, R. Zauel, M.J. Flynn, Y.N. Yeni, Digital tomosynthesis and high resolution computed tomography as clinical tools for vertebral endplate topography measurements: comparison with microcomputed tomography, Bone 81 (2015) 300–305.
[36] D.A. Reimann, S.M. Hames, M.J. Flynn, D.P. Fyhrie, A cone beam computed tomography system for true 3D imaging of specimens, Appl. Radiat. Isot. 48 (10–12) (1997) 1433–1436.
[37] J. Schindelin, I. Arganda-Carreras, E. Frise, V. Kaynig, M. Longair, T. Pietzsch, S. Preibisch, C. Rueden, S. Saalfeld, B. Schmid, J.Y. Tinevez, D.J. White, V. Hartenstein, K. Eliceiri, P. Tomancak, A. Cardona, Fiji: an open-source platform for biological-image analysis, Nat. Methods 9 (7) (2012) 676–682.
[38] W. Niblack, An Introduction to Digital Image Processing, Prentice-Hall International, Englewood Cliffs, N.J, 1986.
[39] D. Oravec, W. Kim, M.J. Flynn, Y.N. Yeni, The relationship of whole human vertebral body creep to geometric, microstructural, and material properties, J. Biomech. 73 (2018) 92–98.
[40] A. Karperien, FracLac for ImageJ, version 2.5. http://rsb.info.nih.gov/ij/plugins/fraclac/FLHelp/Introduction.htm. 1999-2007, (2007).
[41] N.L. Fazzalari, I.H. Parkinson, Fractal dimension and architecture of trabecular bone, J. Pathol. 178 (1) (1996) 100–105.
[42] D. Chappard, E. Legrand, B. Haettich, G. Chales, B. Auvinet, J.P. Eschard, J. P. Hamelin, M.F. Basle, M. Audran, Fractal dimension of trabecular bone: comparison of three histomorphometric computed techniques for measuring the architectural two-dimensional complexity, J. Pathol. 195 (4) (2001) 515–521.
[43] R.E. Plotnick, R.H. Gardner, R.V. Oneill, Lacunarity indexes as measures of landscape texture, Landsc. Ecol. 8 (3) (1993) 201–211.
[44] S. Baim, C.R. Wilson, E.M. Lewiecki, M.M. Luckey, R.W. Downs Jr., B.C. Lentle, Precision assessment and radiation safety for dual-energy X-ray absorptiometry: position paper of the International Society for Clinical Densitometry, J. Clin. Densitom. 8 (4) (2005) 371–378.
[45] D. Okkalides, M. Fotakis, Patient effective dose resulting from radiographic examinations, Br. J. Radiol. 67 (798) (1994) 564–572.
[46] M.J. Flynn, R. McGee, J. Blechinger, Spatial Resolution of X-ray Tomosynthesis in Relation to Computed Tomography for Coronal/Sagittal Images of the Knee, United states, SPIE, San Diego, CA, 2007 (pp. 65100D-9).
[47] J.T. Dobbins 3rd, D.J. Godfrey, Digital x-ray tomosynthesis: current state of the art and clinical potential, Phys. Med. Biol. 48 (19) (2003) R65–106.
[48] Y. Zhang, X. Li, W.P. Segars, E. Samei, Comparison of patient specific dose metrics between chest radiography, tomosynthesis, and CT for adult patients of wide ranging body habitus, Med. Phys. 41 (2) (2014), 023901.
[49] A. Noel, M.A. Ottenin, C. Germain, M. Soler, N. Villani, O. Grospretre, A. Blum, Comparison of irradiation for tomosynthesis and CT of the wrist, J Radiol 92 (1) (2011) 32–39.
[50] T. Aoki, M. Fujii, Y. Yamashita, H. Takahashi, H. Oki, Y. Hayashida, K. Saito, Y. Tanaka, Y. Korogi, Tomosynthesis of the wrist and hand in patients with rheumatoid arthritis: comparison with radiography and MRI, AJR Am. J. Roentgenol. 202 (2) (2014) 386–390.
[51] A. De Silvestro, K. Martini, A.S. Becker, T.D.L. Kim-Nguyen, R. Guggenberger, M. Calcagni, T. Frauenfelder, Postoperative imaging of orthopaedic hardware in the hand and wrist: is there an added value for tomosynthesis? Clin Radiol 73 (2) (2018) 214 e1–214 e9.
[52] C.E. Kawalilak, J.D. Johnston, W.P. Olszynski, D.A. Leswick, S.A. Kontulainen, Comparison of short-term in vivo precision of bone density and microarchitecture at the distal radius and tibia between postmenopausal women and young adults, J. Clin. Densitom. 17 (4) (2014) 510–517.
[53] K. Engelke, C. Libanati, Y. Liu, H. Wang, M. Austin, T. Fuerst, B. Stampa, W. Timm, H.K. Genant, Quantitative computed tomography (QCT) of the forearm using general purpose spiral whole-body CT scanners: accuracy, precision and comparison with dual-energy X-ray absorptiometry (DXA), Bone 45 (1) (2009) 110–118.
[54] L. Forsen, G.K. Berntsen, H.E. Meyer, G.S. Tell, V. Fonnebo, N.C.R. Group, Differences in precision in bone mineral density measured by SXA and DXA: the NOREPOS study, Eur. J. Epidemiol. 23 (9) (2008) 615–624.
[55] T.L. Mueller, M. Stauber, T. Kohler, F. Eckstein, R. Muller, G.H. van Lenthe, Non-invasive bone competence analysis by high-resolution pQCT: an in vitro reproducibility study on structural and mechanical properties at the human radius, Bone 44 (2) (2009) 364–371.
[56] K. Engelke, B. Stampa, W. Timm, B. Dardzinski, A.E. de Papp, H.K. Genant, T. Fuerst, Short-term in vivo precision of BMD and parameters of trabecular architecture at the distal forearm and tibia, Osteoporos. Int. 23 (8) (2012) 2151–2158.
[57] S. Lee, J.W. Lee, J.W. Jeong, D.S. Yoo, S. Kim, A preliminary study on discrimination of osteoporotic fractured group from nonfractured group using support vector machine, Conf Proc IEEE Eng Med Biol Soc 2008 (2008) 474–477.
[58] B.C. Hanusch, S.P. Tuck, R.J.Q. McNally, J.J. Wu, M. Prediger, J. Walker, J. Tang, I. Piec, W.D. Fraser, H.K. Datta, R.M. Francis, Does regional loss of bone density explain low trauma distal forearm fractures in men (the Mr F study)? Osteoporos. Int. 28 (10) (2017) 2877–2886.
[59] E. Barrett-Connor, S.G. Sajjan, E.S. Siris, P.D. Miller, Y.T. Chen, L.E. Markson, Wrist fracture as a predictor of future fractures in younger versus older postmenopausal women: results from the National Osteoporosis Risk Assessment (NORA), Osteoporos. Int. 19 (5) (2008) 607–613.

[60] C.J. Crandall, K.M. Hovey, J.A. Cauley, C.A. Andrews, J.R. Curtis, J. Wactawski-Wende, N.C. Wright, W. Li, M.S. LeBoff, Wrist fracture and risk of subsequent fracture: findings from the women's health initiative study, J. Bone Miner. Res. 30 (11) (2015) 2086–2095.
[61] S. Niempoog, S. Sukkarnkosol, K. Boontanapibul, Prevalence of osteoporosis in patients with distal radius fracture from low-energy trauma, Malays Orthop J 13 (3) (2019) 15–20.
[62] L. Doo, C.L. Shapiro, Skeletal manifestations of treatment of breast cancer on premenopausal women, Curr Osteoporos Rep 11 (4) (2013) 311–318.
[63] H. Abdel-Razeq, A. Awidi, Bone health in breast cancer survivors, J. Cancer Res. Ther. 7 (3) (2011) 256–263.
[64] J.L. Khatcheressian, P. Hurley, E. Bantug, L.J. Esserman, E. Grunfeld, F. Halberg, A. Hantel, N.L. Henry, H.B. Muss, T.J. Smith, V.G. Vogel, A.C. Wolff, M. R. Somerfield, N.E. Davidson, O. American Society of Clinical, Breast cancer follow-up and management after primary treatment: American Society of Clinical Oncology clinical practice guideline update, J Clin Oncol 31 (7) (2013) 961–965.
[65] E. Senkus, S. Kyriakides, S. Ohno, F. Penault-Llorca, P. Poortmans, E. Rutgers, S. Zackrisson, F. Cardoso, E.G. Committee, Primary breast cancer: ESMO clinical practice guidelines for diagnosis, treatment and follow-up, Ann. Oncol. 26 (Suppl. 5) (2015) v8–30.
[66] J.H. Yoon, M.J. Kim, E.K. Kim, H.J. Moon, Imaging surveillance of patients with breast cancer after primary treatment: current recommendations, Korean J. Radiol. 16 (2) (2015) 219–228.
[67] R.N. Uppot, Technical challenges of imaging & image-guided interventions in obese patients, Br. J. Radiol. 91 (1089) (2018) 20170931.
[68] N. Binkley, D. Krueger, N. Vallarta-Ast, An overlying fat panniculus affects femur bone mass measurement, J. Clin. Densitom. 6 (3) (2003) 199–204.
[69] P. Tothill, W.J. Hannan, S. Cowen, C.P. Freeman, Anomalies in the measurement of changes in total-body bone mineral by dual-energy X-ray absorptiometry during weight change, J. Bone Miner. Res. 12 (11) (1997) 1908–1921.
[70] B.C. Silva, S.B. Broy, S. Boutroy, J.T. Schousboe, J.A. Shepherd, W.D. Leslie, Fracture risk prediction by non-BMD DXA measures: the 2015 ISCD official positions part 2: trabecular bone score, J. Clin. Densitom. 18 (3) (2015) 309–330.
[71] W.D. Leslie, E. Shevroja, H. Johansson, E.V. McCloskey, N.C. Harvey, J.A. Kanis, D. Hans, Risk-equivalent T-score adjustment for using lumbar spine trabecular bone score (TBS): the Manitoba BMD registry, Osteoporos. Int. 29 (3) (2018) 751–758.
[72] W.D. Leslie, B. Aubry-Rozier, L.M. Lix, S.N. Morin, S.R. Majumdar, D. Hans, Spine bone texture assessed by trabecular bone score (TBS) predicts osteoporotic fractures in men: the Manitoba bone density program, Bone 67 (2014) 10–14.